IEEE Photonics Journal
An IEEE Photonics Society Publication

Open Access

Effect of Directional Movement on Dynamic Light Scattering

Volume 13, Number 3, June 2021

Guiqiong Huang
Bingquan Xu
Jian Qiu
Li Peng
Kaiqing Luo
Dongmei Liu
Peng Han

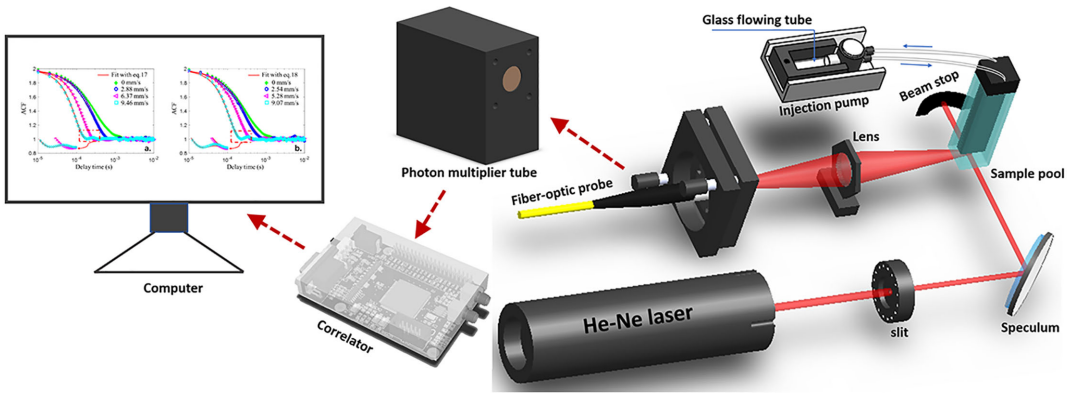

DOI: 10.1109/JPHOT.2021.3083611

Effect of Directional Movement on Dynamic Light Scattering

Guiqiong Huang,[1] Bingquan Xu,[1] Jian Qiu,[1,2] Li Peng,[1,2] Kaiqing Luo,[1,2] Dongmei Liu,[1,2] and Peng Han[1,2]

[1]Guangdong Provincial Engineering Research Center for Optoelectronic Instrument, SPTE, South China Normal University, Guangzhou 510006, China
[2]SCNU Qingyuan Institute of Science and Technology Innovation, Qingyuan 511517, China

DOI:10.1109/JPHOT.2021.3083611

Manuscript received April 14, 2021; revised May 20, 2021; accepted May 21, 2021. Date of publication May 25, 2021; date of current version June 21, 2021. This work was supported in part by the National Natural Science Foundation of China under Grant 61975058, in part by the Natural Science Foundation of Guangdong Province under Grant 2019A1515011401, in part by the Science and Technology Program of Guangzhou under Grant 2019050001, and in part by the Science and Technological Plan of Guangdong Province, China under Grant 2019B090905005. Corresponding author: Peng Han (e-mail: hanp@scnu.edu.cn).

Abstract: Dynamic light scattering is a standard technique of nano-particle sizing in colloid systems. However, it is difficult to measure the particle size accurately in the flowing dispersion, which is inevitable in many applications, such as on-line measurement. In this paper, we present that the wave vector of the scattered light, which is averaged to a constant in traditional technique, varies with time when the particles undergoing not only the random motion but also the directional movement. This variation results in an additional term of sinc function to the traditional intensity autocorrelation function of the scattered light, thus affect the final particle size determination, especially for large velocity of the directional movement. The experimental results agree well with our derivation. We believe this will facilitate the extension of the technique of the dynamic light scattering to a wider range of application, especially of the on-line measurement in the flowing dispersion.

Index Terms: Dynamic light scattering, intensity autocorrelation function, scattering wave vector, directional movement.

1. Introduction

Dynamic light scattering (DLS) is one of the main methods for size measurement of the nanometer and submicron particles in colloid systems [1]–[6]. Due to the random Brownian motion of the particles, the scattered light from the particles interfere with each other, leading to stochastic fluctuation of the scattered light intensity located at the detector [7]. By calculating the intensity autocorrelation function (ACF) of the scattered light, the diffusion coefficient of the particles can be determined by the reversion algorithms [8], [9]. Finally, the particle size can be determined according to Stokes-Einstein function [10], [11]. Since this technique is non-intrusive, quick and accurate, the ISO recommends it as a standard method to size the nanometer and submicron particles in colloids [12], [13].

However, the traditional technique of DLS does not work well when the dispersion is flowing, which is very popular in many applications, such as the on-line measurement system, the inhomogeneity system and etc [14]–[20]. The key of the DLS is the calculation of the intensity ACF of the

scattered light, which represents the degree of the intensity fluctuation and is directly related to the diffusion coefficient and the size of the particles [21]. As mentioned above, the intensity fluctuation at the detector is assumed in DLS to be caused by the random motion of the particles. However, if there are another kinds of particle movement in the dispersion, the meaning of the ACF might be confused [22]–[24].

Initially, researchers believed that the directional movement of the particles did not affect ACF, since the relative distances between the particles were not changed when they moved in the same direction and speed [25]. However, the measured ACFs show obvious difference between static and flowing dispersion. Then some researchers attribute this difference to the Gaussian incident light field. Chowdhury and his colleagues following the work of Edwards et al. [26], have discussed the theory of DLS for a flowing dispersion of Brownian particles. They assumed a spherically symmetric Gaussian incident beam with a plane wave front in the scattering volume [27]. Subsequently, Taylor and Sorensen extended the theory of DLS for a flowing dispersion of diffusing particles to include the Gaussian shape properties of an incident light beam. They showed the effect of Gaussian beams on the correlation functions from flowing Brownian motion systems [28]. Weber et al. developed an analytical expression for the homodyne autocorrelation function of laser light scattered by a laminar flow of a polydisperse particle-fluid system [29]. Overall, these published works assume that the profile of the actual incident light follows the Gaussian distribution, so the scattered light will change when the particles move in the direction not parallel with the incident light. The final expression of the ACF contains an additional exponential function that is related to the beam-waist radius of the incident light and the velocity of the particles. However, the sample volume is generally limited to a scale of 0.1 mm by the slit to ensure the spatial coherence in many classical DLS experiments. Therefore, the incident light is more like a uniform beam.

We present that the change of the scattering wave vector should be included in the ACF when particles undergo random motion and directional movement simultaneously. In traditional technique of DLS, the averaged scattering wave vectors of the particles are assumed to be invariant since the particles move randomly. However, when the particles move in the same direction, the scattering wave vector of all particles change in the same way. The change of the wave vector means the variance of the optical path difference of the scattered light, so the light intensity will change accordingly. This intensity change can be easily detected since the sampling time of the detector (several micro-second in general) is shorter than the time interval of the particle traveling through the incident light beam. So the ACF calculated from the intensity fluctuation of the scattered light contains information of both random motion and directional movement of the particles.

In this paper, we derived the intensity ACF of the scattered light of the particles in flowing dispersion. In contrast to the traditional ACF that is a superposition of weighted exponential functions, there is an additional term of sinc function related to the velocity of the directional movement. This term accelerates the decay of the ACF obviously, especially for relative large velocity of the directional movement. The derived ACFs agree well with the experimental results and have higher R-squared than the existing Gaussian model, contributing to more accurate calculated particle size. We believe our model can describe the dynamic light scattering from particle systems more accurately, and will facilitate the extension of the application of the DLS, especially for the on-line measurement in the flowing dispersion.

2. Principle and Method

Supposing ϕ_{jd} and ϕ_{jc} are the phase of the jth particle caused by random motion and directional movement respectively, the scattered light electric field $E(\mathrm{t})$ is [29]

$$E(t) = E_0 \sum_{j=1}^{N} \exp\left\{i\left[\phi_{jd}(t) + \phi_{jc}(t) - \omega_0 t\right]\right\}, \tag{1}$$

where E_0, N and ω_0 are the electric field at the observation point, the number of particles and the frequency respectively. Then the intensity of the scattered light $I(t)$ [30],

$$I(t) = E(t)E^*(t) = E_0^2 \sum_{j=1}^{N} \sum_{k=1}^{N} \exp\left\{i\left[\phi_{jd}(t) - \phi_{kd}(t) + \phi_{jc}(t) - \phi_{kc}(t)\right]\right\}. \tag{2}$$

The ACF of the scattered light intensity $G_2(\tau)$ is given by

$$G_2(\tau) = \langle I(t)\, I(t+\tau)\rangle. \tag{3}$$

Substituting Eq. (1) and (2) into Eq. (3), $G_2(\tau)$ can be obtained:

$$G_2(\tau) = \left\langle E_0^4 \sum_{j=1}^{N}\sum_{k=1}^{N}\sum_{l=1}^{N}\sum_{m=1}^{N} e^{i\left[\phi_{jd}(t)-\phi_{kd}(t)\right]} e^{-i\left[\phi_{ld}(t+\tau)-\phi_{md}(t+\tau)\right]} e^{i\left[\phi_{jc}(t)-\phi_{kc}(t)\right]} e^{-i\left[\phi_{lc}(t+\tau)-\phi_{mc}(t+\tau)\right]} \right\rangle, \tag{4}$$

where j, k, l, m represents different particles, and the jth and the kth particles are supposed to be at time t, whereas the lth and the mth particles are at time $(t+\tau)$. The randomness of the particle positions allows us to simplify the expressions. The terms in Eq. (4) that will not average to zero are those for which 1) j = k and l = m, 2) j = l, k = m, j≠k, 3) j = m, k = l, j≠k. Obviously, the second term is the same as the third term. So $G_2(\tau)$ can be divided into the following two terms that are discussed separately as follows:

$$G_2(\tau) = R_1(\tau) + R_2(\tau). \tag{5}$$

1) The first term (j = k, l = m),

$$R_1(\tau) = \left\langle E_0^4 \sum_{j=1}^{N}\sum_{j=1}^{N}\sum_{l=1}^{N}\sum_{l=1}^{N} e^{i\left[\phi_{jd}(t)-\phi_{jd}(t)\right]} e^{-i\left[\phi_{ld}(t+\tau)-\phi_{ld}(t+\tau)\right]} e^{i\left[\phi_{jc}(t)-\phi_{jc}(t)\right]} e^{-i\left[\phi_{lc}(t+\tau)-\phi_{lc}(t+\tau)\right]} \right\rangle. \tag{6}$$

This term shows the correlation of the particle and itself. So $R_1(\tau)$ is given by

$$R_1(\tau) = E_0^4 N^2. \tag{7}$$

1) The second term (j = l, k = m, j≠k),

$$R_2(\tau) = \left\langle E_0^4 \sum_{j=1}^{N}\sum_{k=1}^{N}\sum_{j=1}^{N}\sum_{k=1}^{N} e^{i\left[\phi_{jd}(t)-\phi_{jd}(t+\tau)\right]} e^{-i\left[\phi_{kd}(t)-\phi_{kd}(t+\tau)\right]} e^{i\left[\phi_{jc}(t)-\phi_{jc}(t+\tau)\right]} e^{-i\left[\phi_{kc}(t)-\phi_{kc}(t+\tau)\right]} \right\rangle. \tag{8}$$

This term shows the correlation between the particle and itself after delay time τ. When the particles are in the flowing dispersion, the movements of the particles can be decomposed into two averages: one over the random motion and the other over the directional movement. Since the two movements are independent of each other, $R_2(\tau)$ can be divided into the product of the two averages [27]–[29]:

$$R_2(\tau) = \left\langle E_0^4 \sum_{j=1}^{N}\sum_{k=1}^{N}\sum_{j=1}^{N}\sum_{k=1}^{N} e^{i\left[\phi_{jd}(t)-\phi_{jd}(t+\tau)\right]} e^{-i\left[\phi_{kd}(t)-\phi_{kd}(t+\tau)\right]} \right\rangle \left\langle e^{i\left[\phi_{jc}(t)-\phi_{jc}(t+\tau)\right]} e^{-i\left[\phi_{kc}(t)-\phi_{kc}(t+\tau)\right]} \right\rangle. \tag{9}$$

The average over random motion gives an exponential decay function [27], [28], so $R_2(\tau)$ can be simplified as

$$R_2(\tau) = E_0^4 N(N-1)\, e^{-2\Gamma\tau} \left\langle \exp\left\{i\left[\phi_{jc}(t) - \phi_{jc}(t+\tau)\right]\right\} \exp\left\{-i\left[\phi_{kc}(t) - \phi_{kc}(t+\tau)\right]\right\} \right\rangle, \tag{10}$$

where Γ is the decay constant due to random motion of the particles in the sample volume.

In order to calculate the average over directional movement, the sample volume should be clarified. Fig. 1(a) shows the profile of the sample volume region in our model, and Fig. 1(b) and (c) give the two aspects according to its direction parallel or vertical to the incident light, respectively.

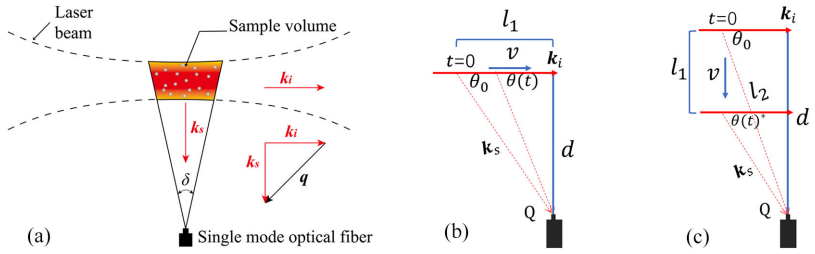

Fig. 1. (a) Detail of the sample volume region. The red shaded area represents the sample volume. δ is determined by the numberical aperture of the single mode optical fiber. (b) Optical diagram of parallel field. (c) Optical diagram of vertical field.

The scattered light is collected by a single mode fiber as denoted by Q. The scattering angle of the particle is θ_0 at time t = 0 and θ(t) at time t. ν is the directional velocity. $\mathbf{k}_i$ and $\mathbf{k}_s$ are the wave vector of incident light and scattered light, respectively. d is the vertical distance between the scattering position and the fiber. l_1 is the length of sample volume. In Fig. 1(c), l_2 is the distance between the scattering position and the detector.

The scattering wave vector $q = \mathbf{k}_i - \mathbf{k}_s$ has magnitude

$$q(t) = \frac{4\pi n}{\lambda} \sin\left(\frac{\theta(t)}{2}\right), \tag{11}$$

where n and λ are the medium refractive index and wavelength, respectively. In Fig. 1(b), the scattering angle

$$\theta(t) = \frac{\nu}{d} t + \theta_0. \tag{12}$$

The derivation of Eq. (12) is given in Appendix A. So the phase $\phi(t)$ is given by

$$\phi(t) = q(t) * \nu t = \frac{4\pi n\nu}{\lambda} \sin\left(\frac{\nu t + \theta_0 d}{2d}\right) * t. \tag{13}$$

Combining Eq. (13), the Eq. (10) is given by

$$R_2(\tau) = E_0^4 N(N-1) \exp(-2\Gamma\tau) \left\langle \exp\left\{ i2f\nu t \sin\left({}^{\nu\tau}/_{4d}\right) \cos\left(\frac{2\nu t + \nu\tau + 2\theta_0 d}{4d}\right)\right\}\right\rangle^2. \tag{14}$$

Here, $f = 4\pi n/\lambda$ is the coefficient factor. According to Euler's formula, the Eq. (14) can be decomposed into two terms: real and imaginary part, and the integral of the imaginary part is zero because it's symmetric to the coordinate axis. thus

$$\begin{aligned} R_2(\tau) &= E_0^4 N(N-1) \exp(-2\Gamma\tau) \left\langle \cos\left[2f\nu t \sin\left({}^{\nu\tau}/_{4d}\right) \cos\left(\tfrac{2\nu t+\nu\tau+2\theta_0 d}{4d}\right)\right]\right\rangle^2 \\ &\approx E_0^4 N(N-1) \exp(-2\Gamma\tau) \sin c^2\left({}^{\sqrt{2}\pi n l_1 \nu\tau}/_{\lambda d}\right). \end{aligned} \tag{15}$$

The detailed calculation process of Eq. (15) is given in Appendix B. Then ACF $G_2(\tau)$ is given by

$$G_2(\tau) = R_1(\tau) + R_2(\tau) = E_0^4 N^2 + E_0^4 N(N-1) \exp(-2\Gamma\tau) \sin c^2\left({}^{\sqrt{2}\pi n l_1 \nu\tau}/_{\lambda d}\right). \tag{16}$$

Since N is generally large, the ACF can be normalized to

$$g_2(\tau) = 1 + \exp(-2\Gamma\tau) \sin c^2\left({}^{\sqrt{2}\pi n l_1 \nu\tau}/_{\lambda d}\right). \tag{17}$$

This is different with the ACF of the traditional DLS technique, where $g_2(\tau) = 1 + \exp(-2\Gamma\tau)$. It can be seen that due to the existence of the directional movement, the ACF is not just an

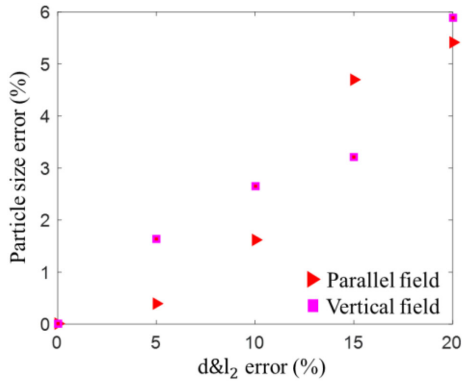

Fig. 2. Experimental results diagram: relationship between the particle size error and the distance error for the parallel and vertical case, respectively.

TABLE 1
Key Parameters in Eq.(17) and Eq.(18)

Particle size (nm)	Decay constant (s^{-1})	Medium refractive index	Sample volume (mm^2)	Directional velocity (mm/s)	Wavelength (nm)	Distance d&l_2 (m)
100	1708.9	1.33	0.5*0.5	1.0	632.8	0.15

exponential decay function but multiplied by a sinc function, which will accelerate the decay of the ACF curve, especially at large time interval. Notice that the distance between the scattering position and the fiber should be measured. We verified the effect of distance error: table1 shows the key parameters and Fig. 2 shows the relationship between the particle size error and the distance error. It can be seen that if the particle size error is to be within 5%, then the distance error must be within 15%, which is relatively easy to be satisfied.

As for vertical fields in Fig. 1(c), the result is very similar:

$$g_2'(\tau) = 1 + \exp(-2\Gamma\tau)\sin c^2\left(\sqrt{2}\pi n l_1 \nu\tau \Big/ \lambda l_2\right). \tag{18}$$

Except that d in Eq. (17) is replaced l_2 by in Eq. (18), since the scattering angle in Fig. 1(c) is

$$\theta(t)^* = -\frac{\nu}{l_2}t + \theta_0. \tag{19}$$

Fig. (3) shows the calculated ACF of 100nm particles at different velocities according to the Eq. (17) and (18). It can be seen that with the increase of the velocity, the curves attenuate faster. In addition, the oscillations are observed near the baseline of the ACF, especially for large velocity of the directional movement.

3. Experimental and Discussion

A suspension of monodisperse polystyrene latex spheres in water has through the years provided a convenient and simple system with which to ensure the proper working of a DLS experiment [26]–[27]. Here we again use this system only now providing a variable uniform flow speed to test the theoretical expression above. The suspension was purchased from BS-Partikel GmbH. The nominal size of the particle is 100 nm, and its approximate concentration is 2.0%. The microsphere density is 1.05 g/mL, and its index of refraction is 1.59@589 nm, and the rel. standard dev. (C.V.) is 4.7%. The suspension was divided in triplicate (Sample 1, Sample 2 and Sample 3), and was

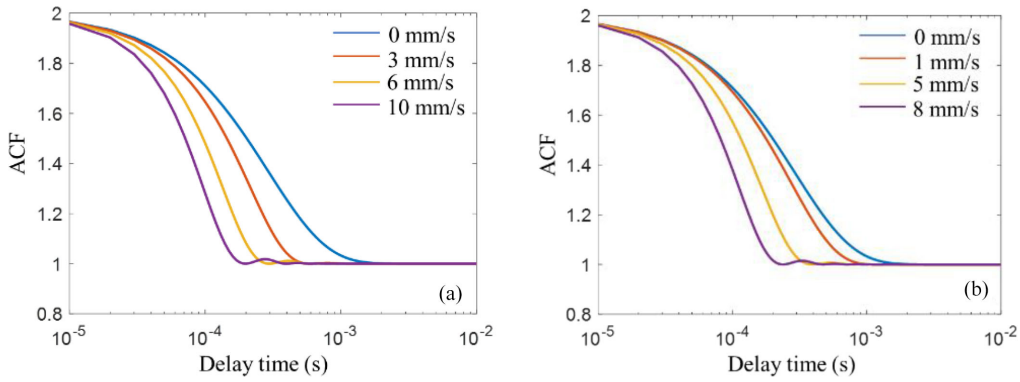

Fig. 3. (a) The normalized ACF of parallel field. (b) The normalized ACF of vertical field.

TABLE 2
Results for the Measurement of Particle Size

Sample	Nominal size (nm)	Measured size(nm)	Error(%)
1	100	99.6	0.40
2	100	98.2	1.80
3	100	102.3	2.30

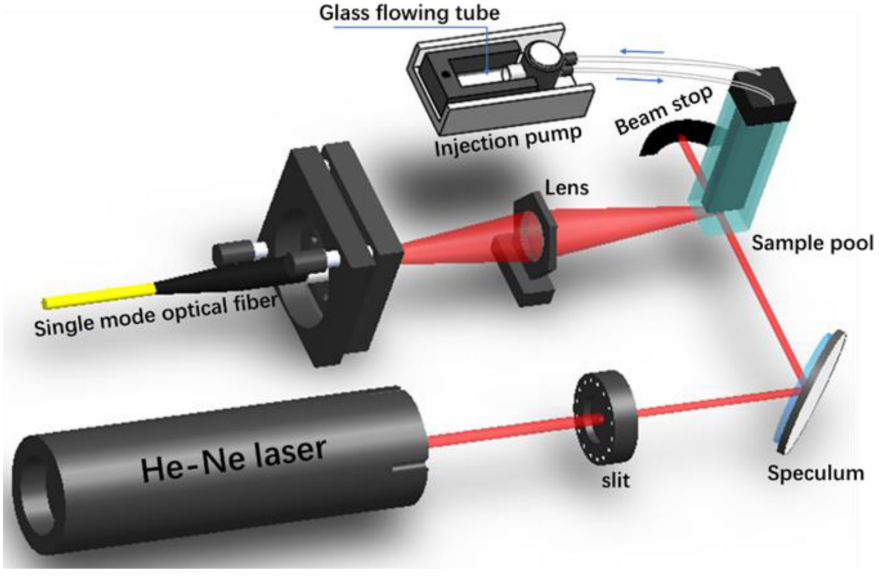

Fig. 4 Optical arrangement diagram at directional velocity.

measured by a commercial instrument [Micromeritics (NanoPlus HD zeta/nano particle analyzer)]. Table 2 shows the results.

The optical arrangement, as shown in Fig. 4, comprises a He-Ne laser, an adjustable slit, sample pool, an injection pump (MSP1-E1, LONGER, U.K.) [30], lens imaging system, a single mode optical fiber (GCX-XSM-4, DHC, CHN), and a photon correlator (OLAB-C3, HUAAO, CHN). A He-Ne laser of 632.8 nm wavelength is used as the incident light source, while a photon correlator is used as the data processing system. The focal length of the lens is 50.8 mm. A single mode

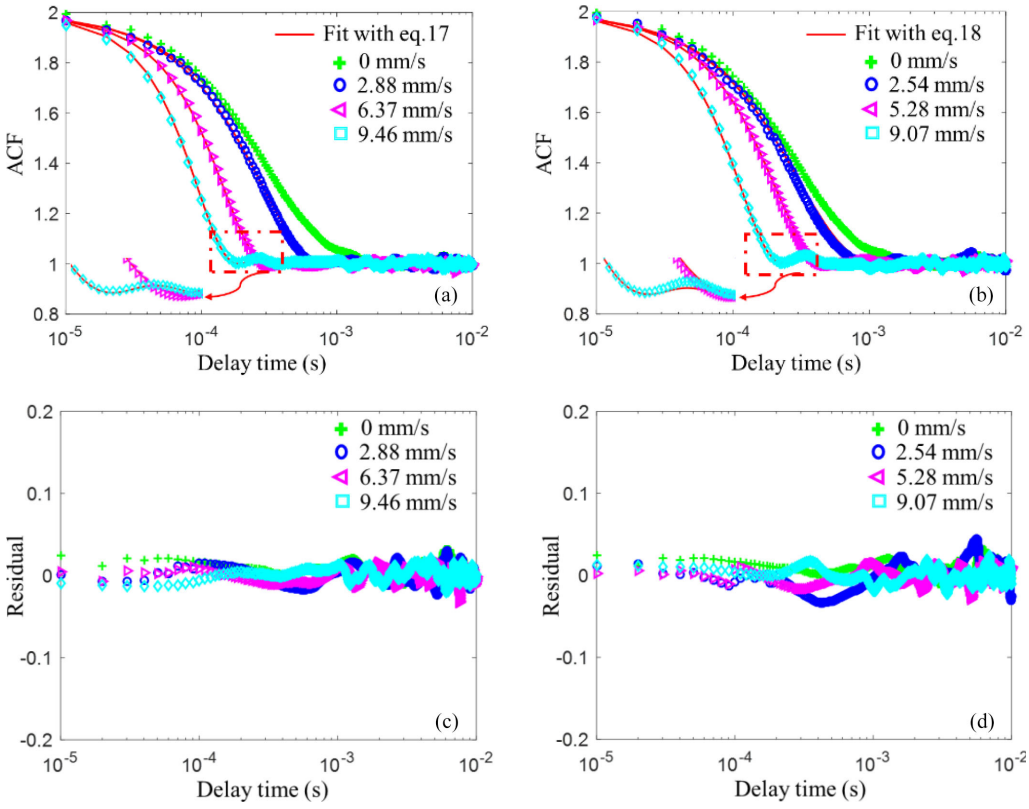

Fig. 5. ACF under different velocities for (a) the parallel case, i.e., the direction of the velocity is parallel with that of the incident light, and (b) the vertical case. The theoretical and experimental results are represented by lines and scatters, respectively. (c) and (d) show the residual plots for ACF data of the parallel case and the vertical case respectively.

optical fiber is used to collect the scattered light and is located slightly behind the image plane of the sample volume.

An injection pump is used to control the uniform flow of the sample liquid. The full volume of the glass flowing tube of the pump is 0.5 mL, and the profile of the sample cell is 25 mm^2, so the velocity of the particle in the sample cell at the measurement point can be adjusted within the range of 0∼20 mm/s. Before each experiment, the sample cell and the entire pipeline system were flushed in two directions with deionized ultrafiltered water for 30 minutes to remove any pollutants (such as impurities in previous experiments).

The dispersion was measured under three different velocities in each case, and the results has been shown in Fig. 5(a) and (b). Fig. 5(a) shows the normalized ACF of the dispersion with the flow direction parallel with that of the incident light, while Fig. 5(b) shows the results of the vertical case.

It can be seen that the experimental results agree well with the theoretical ones. As for small velocity, the ACF curve is affected little. However, the ACF curves decay faster with the increase of the flow speed. Furthermore, the baseline of the ACF shows obvious oscillation for the large speed, which is fitted well by our sinc model.

Furthermore, we fitted the experimental results to the Gaussian model [26]–[29], where the ACF is given by

$$g^2(\tau) = 1 + \exp(-2\Gamma\tau)\exp\left(-\frac{v^2\tau^2}{\omega^2}\right), \tag{20}$$

with ω the beam-waist radius of the incident light.

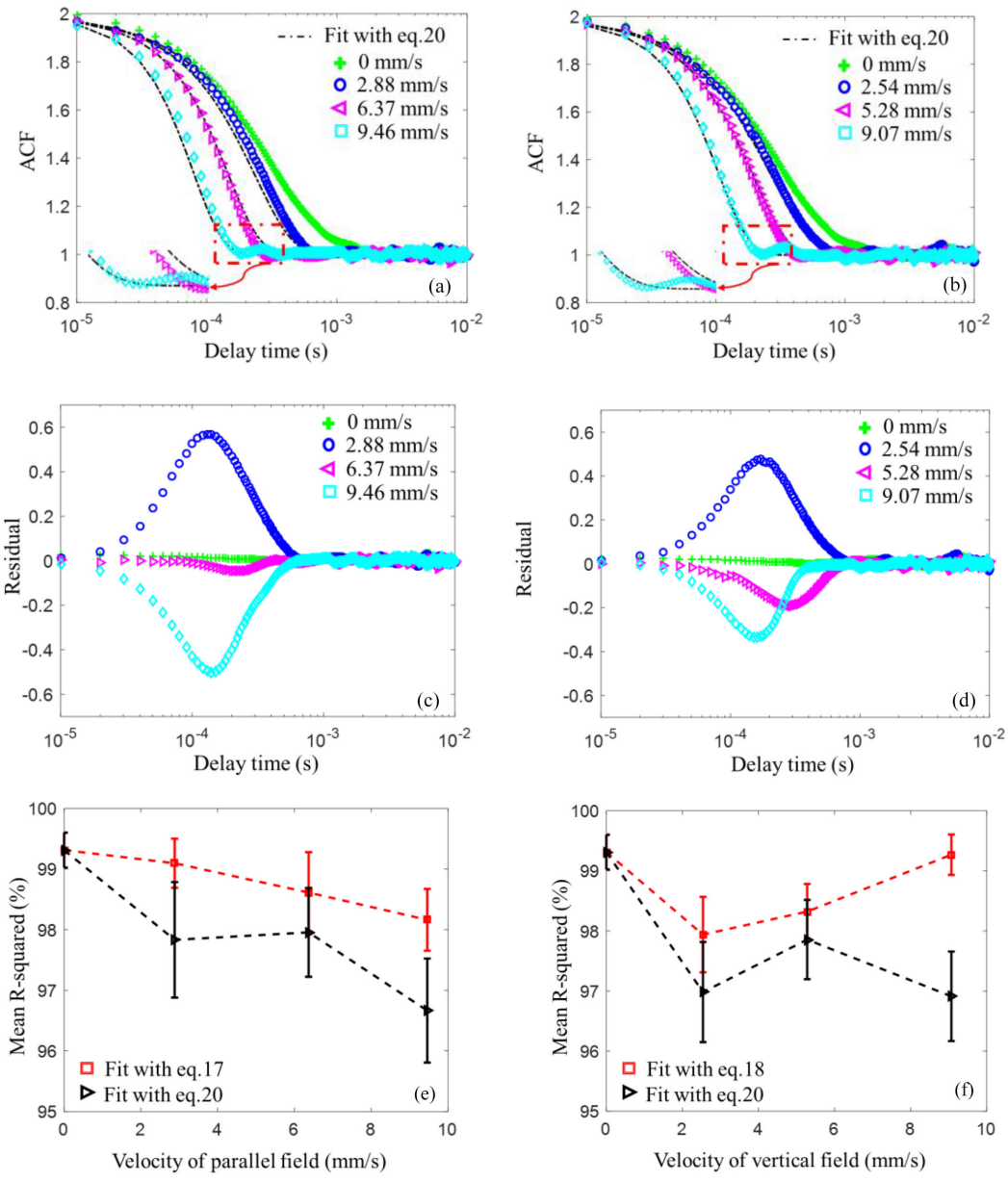

Fig. 6. Gaussian model ACF under different velocities for (a) the parallel case and (b) the vertical case. (c) and (d) show the residual plots for ACF data of the parallel case and the vertical case respectively. (e) and (f) show the R-squared fitted with function Eq. 17, Eq. 18 and Eq. 20 respectively. Each experiment result represents the result of five repeated determinations on the same standard at an appropriate concentration.

Fig. 6(a) and (b) show the fitting of experimental results by Gaussian model for parallel and vertical case, respectively. It is not surprised that the oscillation part of the baseline is not fitted, since the Gaussian model shown in Eq. 20 cannot give that oscillation. As can be seen from Fig. 5 and Fig. 6, the residues in the sinc model are closer value to 0 than Gaussian model, which give a suggestion that our sinc model is better than Gaussian model. To make a better comparison, the R-squared of the sinc model and the Gaussian model are shown in Fig. 6(e) and (f). Indeed, all the

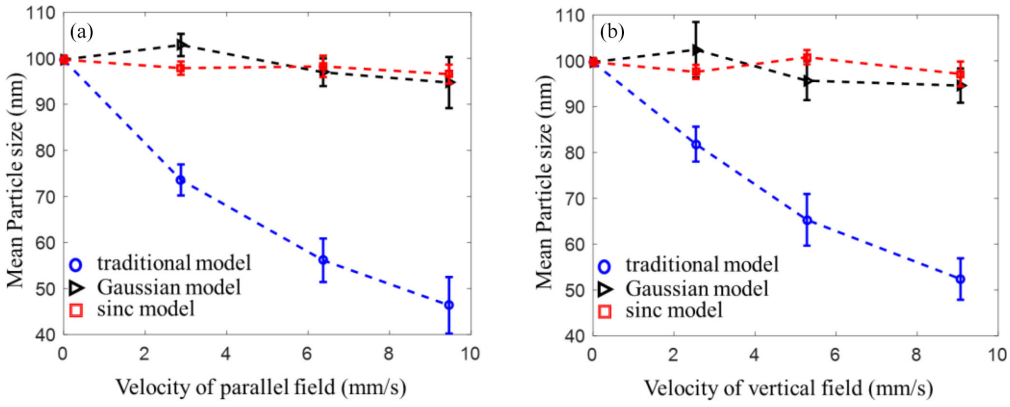

Fig. 7. Relationship between calculated particle size and velocity for (a) the parallel case and (b) the vertical case.

R-squared in the sinc model are higher than those in the Gaussian model, which demonstrate the higher accuracy of the sinc model.

Finally, we fitted the experimental results by different models, i.e., traditional model, Gaussian model and sinc model, and inversed the particle size according to Stokes-Einstein function. The results are shown in the Fig. 7. It can be seen that in the flowing dispersion, the size calculated by the traditional DLS model deviate obviously from the true value, whereas those of both the Gaussian model and our sinc model are still close. Combining with the fitting results of the oscillation part in the baseline of the ACF as mentioned above, we believe our sinc model is more accurate than Gaussian model in our experiments.

4. Conclusion

In this paper, we present a sinc model to describe the ACF of the scattered light from the particle systems undergoing random motion and directional movement simultaneously. In contrast to the traditional ACF that is a superposition of weighted exponential functions, there is an additional term of sinc function related to the velocity of the directional movement. This term not only accelerates the decay of the ACF obviously but generates the oscillation of the baseline of the ACF. Our model agrees well with the experimental results and have higher R-squared than the existing Gaussian model. We believe this work can improve the accuracy of the DLS technique and extend its application, especially in on-line measurement.

Appendix

Appendix A: the scattering angle function

In order to prove the equality of Eq. (12), we first introduce the Taylor series [31]

$$\begin{aligned} \tan x &= x + \tfrac{x^3}{3} + \tfrac{2x^5}{15} + \ldots + \tfrac{2^{2n}\left(2^{2n}-1\right)}{(2n)!}, \\ \sin x &= x - \tfrac{x^3}{3!} + \tfrac{x^5}{5!} \pm \ldots (-1)^n \tfrac{x^{2n+1}}{(2n+1)!}. \end{aligned} \tag{A.1}$$

If x is small, these series show that approximate values are $\tan x \approx x$, $\sin x \approx x$, where, as in the two expansions above, x muse be expressed in radians. The numerical aperture of a single mode optical fiber is extremely small ($NA \approx 0.14$). Thus, in Fig. 1.(b),

$$\tan\left(\frac{\pi}{2} - \theta\left(t\right)\right) \approx \frac{\pi}{2} - \theta\left(t\right). \tag{A.2}$$

According to the geometrical relation,

$$\tan\left(\frac{\pi}{2}-\theta\left(t\right)\right)=\frac{l_1-\nu t}{d}. \tag{A.3}$$

Combining Eq. (A.2) and (A.3),

$$\theta\left(t\right)=\frac{\pi}{2}-\frac{l_1}{d}+\frac{\nu}{d}*t, \tag{A.4}$$

where

$$\frac{l_1}{d}=\tan\left(\frac{\pi}{2}-\theta_0\right)\approx\frac{\pi}{2}-\theta_0. \tag{A.5}$$

So the scattering angle functionθ(t) is given by

$$\theta\left(\mathrm{t}\right)=\frac{\nu}{\mathrm{d}}t+\theta_0. \tag{A.6}$$

Appendix B: the calculation process of the second term $R_2(\tau)$

Here we solve Eq. (15) exactly for the second term: j=l, k=m, j≠k. We discuss the phase difference part of the jth particle and now use Eq. (11) and Eq. (A.6) to calculate the scattering wave vector at time t and $(t+\tau)$, respectively. We can write them as

$$q\left(t\right)=2a*\sin\left(\frac{kt+\theta_0}{2}\right), \tag{B.1}$$

$$q\left(t+\tau\right)=2a*\sin\left(\frac{k\left(t+\tau\right)+\theta_0}{2}\right), \tag{B.2}$$

where

$$a=\frac{2\pi n}{\lambda}, \tag{B.3}$$

$$k=\frac{\nu}{d}. \tag{B.4}$$

Substitute Eq. (B.1) and Eq. (B.2) into Eq. (13) respectively, we can derive the phase difference function,

$$\begin{aligned}\triangle\phi&=\phi\left(t+\tau\right)-\phi\left(t\right)\\&=2a\left[\sin\left(\frac{k\left(t+\tau\right)+\theta_0}{2}\right)-\sin\left(\frac{kt+\theta_0}{2}\right)\right]*\nu t+2a\sin\left(\frac{k\left(t+\tau\right)+\theta_0}{2}\right)*\nu\tau.\end{aligned} \tag{B.5}$$

Firstly, we consider the jth particle. The exponential term of Eq. (10) can be obtained,

$$\begin{aligned}&\left\langle\exp\left\{i\left[\phi_{jc}\left(t\right)-\phi_{jc}\left(t+\tau\right)\right]\right\}\right\rangle=\left\langle\exp\left(i\triangle\phi_j\right)\right\rangle\\&=\left\langle\exp\left\{i\left[2a\nu t\left[\sin\left(\frac{k\left(t+\tau\right)+\theta_0}{2}\right)-\sin\left(\frac{kt+\theta_0}{2}\right)\right]+2a\nu t\sin\left(\frac{k\left(t+\tau\right)+\theta_0}{2}\right)\right]\right\}\right\rangle.\end{aligned} \tag{B.6}$$

According to trigonometric function [31],

$$\sin x-\sin y=2*\cos\left(\frac{x+y}{2}\right)*\sin\left(\frac{x-y}{2}\right). \tag{B.7}$$

The Eq. (B.6) is given by

$$\left\langle\exp\left(i\triangle\phi_j\right)\right\rangle=\left\langle\exp\left\{i\left[4a\nu t*\sin\left(\frac{k\tau}{4}\right)\cos\left(\frac{2kt+k\tau+2\theta_0}{4}\right)\right]\right\}\right\rangle. \tag{B.8}$$

The Eq. (B.8) can be decomposed into two terms: real and imaginary according to Euler's formula:

$$\begin{aligned}\langle \exp(i \triangle \phi_j)\rangle = &\left\langle \cos\left[4a\nu t * \sin\left(\tfrac{k\tau}{4}\right)\cos\left(\tfrac{2kt+k\tau+2\theta_0}{4}\right)\right]\right\rangle \\ &+\left\langle i\sin\left[4a\nu t * \sin\left(\tfrac{k\tau}{4}\right)\cos\left(\tfrac{2kt+k\tau+2\theta_0}{4}\right)\right]\right\rangle.\end{aligned} \tag{B.9}$$

And the integral of the imaginary part is zero because it's symmetric to the coordinate axis,

$$\langle \exp(i \triangle \phi_j)\rangle = \left\langle \cos\left[4a\nu t * \sin\left(\frac{k\tau}{4}\right)\cos\left(\frac{2kt+k\tau+2\theta_0}{4}\right)\right]\right\rangle \tag{B.10}$$

Substitute Eq. (B.3) and Eq. (B.4) into Eq. (B.10), we can get the following identity,

$$\langle \exp(i \triangle \phi_j)\rangle = \left\langle \cos\left[4 * \frac{2\pi n}{\lambda} * \nu t * \sin\left(\frac{\nu\tau}{4d}\right)\cos\left(\frac{2\nu t+\nu\tau+2\theta_0 d}{4d}\right)\right]\right\rangle. \tag{B.11}$$

Let $f = 4\pi n/\lambda$, we obtain

$$\langle \exp(i \triangle \phi_j)\rangle = \left\langle \cos\left[2f\nu t * \sin\left(\frac{\nu\tau}{4d}\right)\cos\left(\frac{2\nu t+\nu\tau+2\theta_0 d}{4d}\right)\right]\right\rangle. \tag{B.12}$$

Note that the same exponential term is found for the kth particle due to the particle independence,

$$\langle \exp(i \triangle \phi_k)\rangle = \left\langle \cos\left[2f\nu t * \sin\left(\frac{\nu\tau}{4d}\right)\cos\left(\frac{2\nu t+\nu\tau+2\theta_0 d}{4d}\right)\right]\right\rangle. \tag{B.13}$$

Therefore, the $R_2(\tau)$ in Eq. (10) is given by

$$R_2(\tau) = E_0^4 N(N-1)\exp(-2\Gamma\tau)\left\langle \cos\left[2f\nu t * \sin\left(\frac{\nu\tau}{4d}\right)\cos\left(\frac{2\nu t+\nu\tau+2\theta_0 d}{4d}\right)\right]\right\rangle^2. \tag{B.14}$$

Next, we define

$$F_1 = \cos\left[2f\nu t * \sin\left(\frac{\nu\tau}{4d}\right)\cos\left(\frac{2\nu t+\nu\tau+2\theta_0 d}{4d}\right)\right]. \tag{B.15}$$

In the classical DLS experiments, the unit of sampling time τ is *us*, the distance d between the scattering position and the fiber is *cm*, and the directional velocity ν is *mm/s* [30], [32]. For simplicity, we assume that $\tau = 10^{-5}$s, $d = 0.15$m, and $\nu = 1 * 10^{-3}$m/s, so

$$\frac{\nu\tau}{4\mathrm{d}} = \frac{1*10^{-3}*10^{-5}}{4*0.15} = 1.6*10^{-8} \ll \frac{\theta_0}{2}. \tag{B.16}$$

Therefore, we can ignore the factor $\nu\tau/4d$. Then

$$\begin{aligned}F_1 &= \cos\left[2f\nu t * \sin\left(\tfrac{\nu\tau}{4d}\right)\cos\left(\tfrac{\nu t}{2d}+\tfrac{\theta_0}{2}\right)\right] \\ &= \cos\left[\zeta t * \cos\left(\tfrac{\nu t}{2d}+\tfrac{\theta_0}{2}\right)\right],\end{aligned} \tag{B.17}$$

where

$$\zeta = 2f\nu\sin\left(\frac{\nu\tau}{4d}\right). \tag{B.18}$$

According to Fig. 1(b),

$$\frac{\nu t}{d} = \tan\left(\frac{\pi}{2}-\theta_0\right) \approx \frac{\pi}{2}-\theta_0, \tag{B.19}$$

since $\frac{\pi}{2}-\theta_0$ is very small. So

$$F_1 = \cos\left(\frac{\sqrt{2}}{2}\zeta * t\right). \tag{B.20}$$

And the average in Eq. (B.14) becomes

$$\begin{aligned}\langle F_1\rangle &= \left\langle \cos\left(\tfrac{\sqrt{2}}{2}\zeta * t\right)\right\rangle \\ &= \lim_{T\to\infty}\frac{\int_0^T \cos\left(\frac{\sqrt{2}}{2}\zeta * t\right)dt}{T} = \frac{\sin\left(\frac{\sqrt{2}}{2}\zeta T\right)}{\frac{\sqrt{2}}{2}\zeta T} = \sin c\left(\tfrac{\sqrt{2}}{2}\zeta T\right) \\ &= \sin c\left(\tfrac{\sqrt{2}\pi n l_1 \nu\tau}{\lambda d}\right),\end{aligned} \tag{B.21}$$

where $\sin(\frac{\nu\tau}{4d}) \approx \frac{\nu\tau}{4d}$, and $T\nu = l_1$.

So, the $R_2(\tau)$ in Eq. (10) is given by

$$R_2(\tau) = E_0^4 N(N-1)\exp(-2\Gamma\tau)\sin c^2\left(\frac{\sqrt{2}\pi n l_1 \nu\tau}{\lambda d}\right). \tag{B.22}$$

Finally, the ACF $G_2(\tau)$ in Eq. (16) is given by

$$G_2(\tau) = R_1(\tau) + R_2(\tau) = E_0^4 N^2 + E_0^4 N(N-1)\exp(-2\Gamma\tau)\sin c^2\left(\frac{\sqrt{2}\pi n l_1 \nu\tau}{\lambda d}\right). \tag{B.23}$$

References

[1] Y. Xu, S. Jin, X. Min, W. Fanyan, and X. Sun, "Deviation-weighted inversion of dynamic light scattering based on autocorrelation function reconstruction," *Acta Optica Sinica*, vol. 38, no. 12, pp. 122–131, 2018.

[2] X. Zhu, J. Shen, and L. Song, "Accurate retrieval of bimodal particle size distribution in dynamic light scattering," *IEEE Photon. Technol. Lett.*, vol. 28, no. 3, pp. 311–314, Feb. 2015.

[3] Y. Wu, W. Yang, C. Wang, J. Hu, and S. Fu, "Chitosan nanoparticles as a novel delivery system for ammonium glycyrrhizinate," *Int. J. Pharmaceutics*, vol. 295, no. 1-2, pp. 235–245, 2005.

[4] S. Pabisch, B. Feichtenschlager, G. Kickelbick, and H. Peterlik, "Effect of interparticle interactions on size determination of zirconia and silicabased systems – A comparison of SAXS, DLS, BET, XRD and TEM," *Chem. Phys. Lett.*, vol. 521, no. 100, pp. 91–97, 2012.

[5] S. Dubin, S. Zietz, K. L. Gabriel, and D. Gabriel, "The mahalanobis distance as a metric in dynamic light scattering particle size analysis: Model studies," in *Proc. IEEE 27th Annu. Northeast Bioeng. Conf.*, Storrs, CT, USA, 2001, pp. 67–68.

[6] J. Shen, J. C. Thomas, X. Zhu, and Y. Wang, "Wavelet denoising experiments in dynamic light scattering," *Opt. Exp.*, vol. 19, no. 13, pp. 12284–12290, 2011.

[7] K. Ishii, T. Iwai, and H. Xia, "Hydrodynamic measurement of Brownian particles at a liquid-solid interface by low-coherence dynamic light scattering," *Opt. Exp.*, vol. 18, no. 7, pp. 7390–7396, 2010.

[8] P. Annelies, A. Ben, and S. Wouter, "Estimation of particle size distributions from bulk scattering spectra: Sensitivity to distribution type and spectral noise," *Opt. Exp.*, vol. 26, no. 12, pp. 15015–15027, 2018.

[9] E. Gulari, E. Gulari, Y. Tsunashima, and B. Chu, "Photon correlation spectroscopy of particle distributions," *J. Chem. Phys.*, vol. 70, no. 8, pp. 3965–3972, 1979.

[10] Z. Li, "Critical particle size where the Stokes-Einstein relation breaks down," *Phys. Rev. E Statal Nonlinear Soft Matter Phys.*, vol. 80, no. 6, pp. 061204–061210, 2009.

[11] Y. Ishii and N. Ohtori, "Molecular insights into the boundary conditions in the Stokes-Einstein relation," *Phys. Rev. E*, vol. 93, no. 5, 2016, Art. no. 050104(R).

[12] L. Wu, "A new measurement method for submicrometer and nanometer particle size analysis-photon correlation spectroscopy," *Shanghai Meas. Testing*, vol. 2, pp. 5–6, 2003.

[13] C. Xu, X. Cai, J. Zhang, and L. Liu, "Fast nanoparticle sizing by image dynamic light scattering," *Particuology*, vol. 19, pp. 82–89, 2015.

[14] C. A. Fraker, A. J. Mendez, L. Inverardi, C. Ricordi, and C. L. Stabler, "Optimization of perfluoro nano-scale emulsions: The importance of particle size for enhanced oxygen transfer in biomedical applications," *Colloids Surfaces B Biointerfaces*, vol. 98, no. 2012, pp. 26–35, 2012.

[15] J. Kim, S. Ahn, H. Lee, and M. Lee, "Estimation of particle size distribution using photon autocorrelation function from dynamic light scattering considering unknown baseline," *Opt. Lett.*, vol. 38, no. 11, pp. 1757–1759, 2013.

[16] P. A. Hassan, S. Rana, and G. Verma, "Making sense of Brownian motion: Colloid characterization by dynamic light scattering," *Langmuir*, vol. 31, no. 1, pp. 3–12, 2015.

[17] L. Karp-Boss, L. Azevedo, and E. Boss, "LISST-100 measurements of phytoplankton size distribution: Evaluation of the effects of cell shape," *Limnol. Oceanogr.: Methods*, vol. 5, no. 11, pp. 396–406, 2007.

[18] W. Schmidt and G. Roessling, "Novel manufacturing process of hollow polymer microspheres," *Chem. Eng. Sci.*, vol. 61, no. 15, pp. 4973–4981, 2006.

[19] T. J. Cho and V. A. Hackley, "Fractionation and characterization of gold nanoparticles in aqueous solution: Asymmetric-flow field flow fractionation with MALS, DLS, and UV–Vis detection," *Anal. Bioanalytical Chem.*, vol. 398, no. 5, pp. 2003–2018, 2010.

[20] J. Gigault and V. A. Hackley, "Differentiation and characterization of isotopically modified silver nanoparticles in aqueous media using asymmetric-flow field flow fractionation coupled to optical detection and mass spectrometry," *Analytica Chimica Acta*, vol. 763, pp. 57–66, 2013.
[21] M. A. Davis and A. K. Dunn, "Dynamic light scattering Monte Carlo: A method for simulating time-varying dynamics for ordered motion in heterogeneous media," *Opt. Exp.*, vol. 13, no. 13, pp. 17145–17155, 2015.
[22] Z. Ma, H. G. Merkus, H. G. V. D. Veen, M. Wong, and B. Scarlett, "On-line measurement of particle size and shape using laser diffraction," *Part. Part. Syst. Characterization*, vol. 18, no. 5/6, pp. 243–247, 2010.
[23] R. Maron, C. O'Keefe, and J. Sepulveda, "Assessing the benefits of automatic grinding control using PST technology for true on-line Particle Size Measurement," *IOP Conf. Ser. Materials Sci. Eng.*, vol. 427, no. 1, pp. 012035–012042, 2018.
[24] Y. Lv, H. Wang, and S. Wei, "The transmission characteristics of indoor particles under two ventilation modes," *Energy Buildings*, vol. 163, no. 2018, pp. 1–9, 2018.
[25] S. Will and A. Leipertz, "Dynamic light scattering system with a novel scattering cell for the measurement of particle diffusion coefficients," *Rev. Sci. Instruments*, vol. 67, no. 9, pp. 3164–3169, 1996.
[26] R. V. Edwards, J. C. Angus, M. J. French, and J. W. Dunning, Jr., "Spectral analysis of the signal from the laser dopper flowmeter: Time-independent systems," *J. Appl. Phys.*, vol. 42, no. 2, pp. 837–850, 1971.
[27] D. P. Chowdhury, C. M. Sorensen, T. W. Taylor, J. F. Merklin, and T. W. Lester, "Application of photon correlation spectroscopy to flowing Brownian motion systems," *Appl. Opt.*, vol. 23, no. 22, pp. 4149–4154, 1984.
[28] T. W. Taylor and C. M. Sorensen, "Gaussian beams effects on the photon correlation spectrum from a flowing Brownian motion system," *Appl. Opt.*, vol. 25, no. 14, pp. 2421–2426, 1986.
[29] R. Weber and G. Schweiger, "Photon correlation spectroscopy on flowing polydisperse fluid-particle systems: Theory," *Appl. Opt.*, vol. 37, no. 18, pp. 4039–4050, 1998.
[30] O. Karal-Yilmaz, E. E. Gurel, N. Kayaman-Apohan, and B. M. Baysal, "Dynamic light scattering," *Tanpakushitsu Kakusan Koso Protein Nucleic Acid Enzyme*, vol. 67, no. 12, pp. 1152–1160,1999.
[31] K. Eriksson, D. Estep, and C. Johnson, *Trigonometric Functions.*, Berlin, Germany: Springer, 2004.
[32] F. Destremaut, J. B. Salmon, L. Qi, and J. P. Chapel, "Microfluidics with on-line dynamic light scattering for size measurements," *Lab A Chip*, vol. 9, no. 22, pp. 3289–3296, 2009.